AD-A154 704 MATRIX FRACTURE IN FIBER-REINFORCED CERAMICS(U) HARVARD 1/1
UNIV CAMBRIDGE MA DIV OF APPLIED SCIENCES
B BUDIANSKY ET AL. MAR 85 MECH-64 N00014-84-K-0510
UNCLASSIFIED F/G 11/2 NL

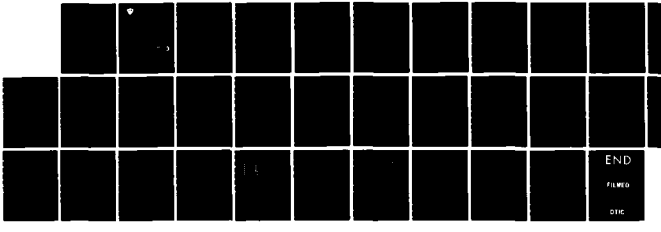

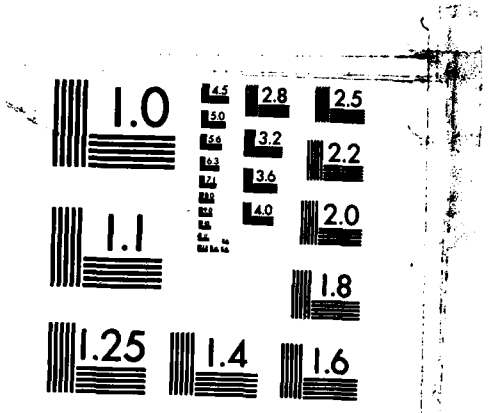

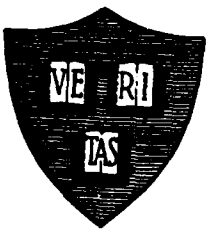

(10)

MECH-64

MATRIX FRACTURE IN FIBER-REINFORCED CERAMICS

Bernard Budiansky, John W. Hutchinson and Anthony G. Evans

Contract N00014-84-K-0510

Division of Applied Sciences
HARVARD UNIVERSITY
Cambridge, Massachusetts 02138

March 1985

MATRIX FRACTURE IN FIBER-REINFORCED CERAMICS

Bernard Budiansky and John W. Hutchinson
Division of Applied Sciences
Harvard University, Cambridge, Massachusetts 02138

Anthony G. Evans
Department of Materials Science and Mining Engineering
University of California, Berkeley, California 94720

ABSTRACT

A fiber-reinforced ceramic subject to tensile stress in the fiber direction can undergo extensive matrix cracking normal to the fibers, while the fibers remain intact. In this paper, the critical conditions for the onset of widespread matrix cracking are studied analytically on the basis of fracture-mechanics theory. Two distinct situations concerning the fiber-matrix interface are contemplated: (i) unbonded fibers initially held in the matrix by thermal or other strain mismatches, but susceptible to frictional slip, and (ii) fibers that initially are weakly bonded to the matrix, but may be debonded by the stresses near the tip of an advancing matrix crack. The results generalize those of the Aveston-Cooper-Kelley theory for case (i). Optimal thermal strain mismatches for maximum cracking strength are studied, and theoretical results are compared with experimental data for a SiC fiber, lithium-alumina-silicate glass matrix composite.

Additional keywords: Stress analysis; computations

NOMENCLATURE

a	fiber radius
c_f, c_m	fiber, matrix volume fractions $(c_f + c_m = 1)$
E	composite Young's modulus, $\approx c_f E_f + c_m E_m$
E_f, E_m	fiber, matrix Young's moduli
μ_m	matrix shear modulus, $= E_m/[2(1+\nu_m)]$

$\mathcal{G}_d$ critical debonding energy-release rate

$\mathcal{G}_m$ critical mode-I matrix energy-release rate

K_m critical mode-I matrix stress-intensity factor $(=\sqrt{E_m \mathcal{G}_m/(1-\nu_m^2)})$

ℓ_d fiber debond length

ℓ_s fiber slip length

q fiber-matrix interface pressure

μ coefficient of friction

ν_f, ν_m fiber, matrix Poisson ratios

τ_s interface slipping shear stress

INTRODUCTION

Fiber-reinforced ceramic materials have promising potential for high-temperature applications (Prewo and Brennan, 1980). Under tensile loading of the composite in the fiber direction, the brittle matrix can undergo extensive cracking normal to the fibers, but the associated matrix cracking stress may be substantially greater than the catastrophic fracture stress of the unreinforced ceramic. Furthermore, with the fibers intact, the composite material can continue to sustain additional load up to the fiber-bundle fracture stress.

This behavior is illustrated by the schematic stress-strain curve shown in Fig. 1. The slope of the initial straight portion of the curve is closely approximated by the rule of mixtures based on matrix and fiber moduli. Extensive matrix cracking, often involving a small stress drop, occurs at A , and the matrix becomes permeated by many, more-or-less equally-spaced cracks that traverse the full cross-section of the specimen. Under continued loading, the fibers alone provide most of the subsequent stiffness. The ultimate strength would ideally be associated with fracture of uniformly strong fibers, but in practice is degraded somewhat as fibers fracture sequentially rather than simultaneously

before the peak stress at B is reached.

In this paper, critical conditions for the onset of widespread matrix cracking are studied theoretically on the basis of fracture-mechanics theory. Two distinct situations concerning the fiber-matrix interfaces are considered: (i) unbonded fibers held in the matrix by initial pressures due to thermal or other strain mismatches, but susceptible to frictional slip, and (ii) fibers under initial radial tension that are weakly bonded to the matrix, but may be debonded by the high stresses near the tip of an advancing matrix crack.

The study of case (i), which generalizes the well-known Aveston-Cooper-Kelly (ACK) theory, (Aveston et al., 1971 ; Aveston and Kelly, 1973; Kelly, 1976; Aveston and Kelly, 1980; Hannant et al., 1983) is based on the analysis of steady-state crack growth in the matrix. The concept adopted (slightly different from that of ACK) is that a "first" planar crack will propagate across the composite under an applied stress that becomes constant during the propagation as soon as the crack engulfs more than a few fibers. With dynamic effects neglected, the stress associated with this steady-state cracking is equivalent to the "first cracking" stress of ACK. (The initiation of growth of the most critical flaw in the matrix could require a somewhat higher stress than that associated with steady-state growth -- hence the slight dip in the stress-strain curve of Fig. 1.) Figure 2 illustrates the matrix crack as it proceeds across the composite. With enough frictional resistance, no slip will occur at the interfaces, as shown in Fig. 2(a). When slip does occur (Fig. 2(b)), the slip length along the fibers on either side of the crack can be expected to approach an asymptotic value on the downstream side of the crack front.

The presumption that Coulomb friction provides the resistance to fiber slip implies that positive fiber-matrix pressures are imposed by strain

mismatches that occur during the fabrication process. It does not however follow that increasing such mismatches would necessarily raise the matrix cracking stress, despite the larger frictional resistance thereby provided. The same strain mismatches also generally lead to initial axial tensile stresses which act to reduce the cracking strength. Accordingly, optimal strain mismatches can be expected to exist, and these will be estimated.

In the case of bonded fibers, the matrix cracking strength will depend on the debonding toughness of the interface. In the presence of sufficiently high debonding toughness, the first matrix crack will propagate in a manner indistinguishable from that of the no-slip frictional case (Fig. 2(a)). If debonding does occur, and the interface pressure is negative (i.e., tensile residual stresses exist between fiber and matrix) the debonded regions will open up, and the crack will propagate as shown in Fig. 2(c). The steady-state cracking calculation will be made for this case on the basis of an elementary analysis of the debonding process near the advancing crack front.

ENERGY RELATIONS

A fairly general relation will be derived for the loss in potential energy of a prestressed elastic body, within which, under constant additional load, cracks develop and open up, and also sliding occurs along internal interfaces. These relations will be used subsequently in the steady-state cracking calculations. Figure 3 shows three states of the body. In state (0), the body is free of external load, but contains an initial tensor stress distribution σ_0 in its volume V. With the external vector tractions T applied to the external boundary S_T in state (1), the stress becomes σ_1, and additional displacements u_1, compatible with additional strains ε_1 are produced. The body may now contain open cracks, as well as internal surfaces in which sliding

has occurred. In state (2), with no change in T, more open cracking has occurred, and additional frictional sliding has taken place along the interface S_F. The final stresses are now σ_2, and the displacements and strains, still measured from the ground state (0), are u_2 and ϵ_2. We want to calculate the potential energy loss $(\pi_1-\pi_2)$ associated with the transition from the energy π_1 in state (1) to π_2 in state (2). The elastic constitutive relations may be written

$$\epsilon = M(\sigma-\sigma_0) \tag{1}$$

for the strain changes produced by σ, where M is a linear operator. Then

$$\pi_0 = \frac{1}{2}\int_V \sigma_0 : M(\sigma_0)dV \tag{2}$$

$$\pi_1 = \frac{1}{2}\int_V \sigma_1 : M(\sigma_1)dV - \int_{S_T} T\cdot u_1 dV \tag{3}$$

$$\pi_2 = \frac{1}{2}\int_V \sigma_2 : M(\sigma_2)dV - \int_{S_T} T\cdot u_2 dV \tag{4}$$

In each case, the volume integral represents the elastic energy stored in the body. Since $\sigma_1 : M(\sigma_2) = \sigma_2 : M(\sigma_1)$, the energy loss may be written as

$$\pi_1 - \pi_2 = \frac{1}{2}\int_V (\sigma_1+\sigma_2) : M(\sigma_1-\sigma_2)dV - \int_{S_T} T\cdot(u_1-u_2)dS \tag{5}$$

We now assume that in state (2), the shear tractions on S_F act in a direction opposite to that of the relative sliding, and have constant magnitude τ_s. Then, by the principle of virtual work,

$$\int_{S_T} T\cdot(u_1-u_2)dS = \int_V \sigma_2 : M(\sigma_1-\sigma_2)dV - \tau_s \int_{S_F} |\Delta v|dS \tag{6}$$

where $|\Delta v|$ is the magnitude of the relative slip on S_F that has occurred during the transition from state (1) to state (2). Hence

$$\pi_1 - \pi_2 = \frac{1}{2}\int_V (\sigma_1-\sigma_2) : M(\sigma_1-\sigma_2)dV + \tau_s \int_{S_F} |\Delta v| dS \qquad (7)$$

If we assume further that slip on S_F has been unvarying and monotonic in direction during the transition to state (2), and that the sliding resistance has always been equal to τ_s, the frictional energy ξ_F dissipated (as heat) is precisely the last integral in (7). Hence

$$\pi_1 - \pi_2 = \frac{1}{2}\int_V (\sigma_1-\sigma_2) : (\varepsilon_1-\varepsilon_2)dV + \xi_F \qquad (8)$$

under the stipulated assumptions. This result is clearly not valid under conditions of variable-direction slip, or history-dependent frictional resistance, during the transition from state (1) to state (2). It does remain correct for pointwise variations in τ_s.

STEADY-STATE CRACKING RELATIONS

To apply the energy relations just developed, we contemplate a long matrix crack of length s in a very wide specimen of width W and unit thickness, as shown in Fig. 4. The crack extends through the thickness of the specimen, with a straight front CC, but all of the fibers are intact. With no change in the average applied stress σ, the crack is presumed to advance an amount Δs to $C'C'$. Now identify the initial uncracked and unloaded but possibly prestressed state of the specimen with state (0), and let the states before and after the crack advance Δs correspond to states (1) and (2). The assumption of steady-state cracking means that the stresses at the crack front, averaged through the thickness, remain unchanged during the crack growth, and also that the upstream and

downstream stress states far ahead of and behind the crack front do not change. Consequently, if we define P_U and P_D as the upstream and downstream potential energies per unit cross sectional area of the composite, it follows that

$$\pi_1 - \pi_2 = (P_U - P_D)\Delta s \tag{9}$$

Hence, the potential energy release rate (per unit crack extension, per unit thickness) is

$$P_U - P_D = \frac{1}{2A_c}\int_{-L}^{L}\int_{A_c}(\sigma_U - \sigma_D) : (\varepsilon_U - \varepsilon_D)\,dA\,dz + \frac{\partial \xi_F}{\partial s} \tag{10}$$

where σ_U , ε_U and σ_D , ε_D are the upstream and downstream stress and strain distributions, and A_c is a representative cross-sectional area of the composite. Here $\frac{\partial \xi_F}{\partial s}$ is the frictional energy dissipation rate (per unit thickness) associated with fiber-matrix slip.

In the case of unbonded, frictionally constrained, slipping fibers, the energy-release rate $P_U - P_D$ must be balanced by the sum of this frictional energy dissipation rate and the critical matrix crack-extension energy-release rate $c_m \mathcal{J}_m$ per unit thickness of the composite. Hence the relation

$$\frac{1}{2A_c}\int_{-L}^{L}\int_{A_c}(\sigma_U - \sigma_D) : (\varepsilon_U - \varepsilon_D)\,dA\,dz = c_m \mathcal{J}_m \tag{11}$$

governs matrix cracking, for both the slip and no-slip cases. If slip does occur, the validity of this result requires that there be monotonically increasing slip along each fiber.

In the case of initially bonded, debonding fibers, the frictional term in (10) is absent, but now a debonding energy release absorbs part of $P_U - P_D$.

For a unit crack advance, the increment in debonded surface area per fiber is $2\pi a\ell_d$ on each side of the crack, and the number per unit area of newly debonded fibers is $c_f/(\pi a^2)$, so that the debonding energy release rate is $4c_f(\ell_d/a)\mathcal{G}$, Hence

$$\frac{1}{2A_c}\int_{-L}^{L}\int_{A_c}(\sigma_U-\sigma_D):(\varepsilon_U-\varepsilon_D)\,dA\,dz = c_m\mathcal{G}_m + 4c_f(\ell_d/a)\mathcal{G}_d \tag{12}$$

In order to implement (11) and (12) for the calculation of the cracking stress, we now have to estimate σ_U and σ_D, and for the debonding situation we also must estimate the debonding length ℓ_d.

FIBER-MATRIX STRESS ANALYSIS

Upstream Stresses

Far ahead of the crack tip, the axial stresses in the fibers and the matrix in the loaded composite are those of the uncracked material. The upstream stresses are therefore well approximated by

$$\left.\begin{aligned}\sigma_f^U &= (E_f/E)\sigma + \sigma_f^I\\ \sigma_m^U &= (E_m/E)\sigma + \sigma_m^I\end{aligned}\right\} \tag{13}$$

where σ is the average applied stress, σ_f^I and σ_m^I are the initial axial stresses in the unloaded composite, and E_f, E_m are the fiber and matrix Young's moduli. This approximation neglects the effects of transverse stresses on axial strains, and is consistent with the rule-of-mixtures expression

$$E = c_fE_f + c_mE_m \tag{14}$$

for the effective axial modulus of the composite. The initial and total stresses satisfy

$$c_f\sigma_f^I + c_m\sigma_m^I = 0 \tag{15}$$

and

$$c_f\sigma_f + c_m\sigma_m = \sigma \tag{16}$$

respectively.

Downstream Stresses

Behind the crack tip, the average fiber and matrix axial stresses at the crack face are

$$\left.\begin{aligned}\sigma_f &= \sigma/c_f \\ \sigma_m &= 0\end{aligned}\right\} \tag{17}$$

and for $L >> a$ the stresses at $z = L$ are given by Eqs. (13). Approximate shear-lag analyses will provide the far-downstream stress distributions in each of the cases shown in Fig. 2.

No-slip case

Far from the crack tip, an isolated composite-cylinder shear-lag model, similar to that adopted by Aveston and Kelly (1973) will be used. Each fiber is presumed to be embedded in a matrix cylinder of outer radius R chosen as

$$R = a/\sqrt{c_f} \tag{18}$$

to provide the correct volume concentration of fibers (Fig. 5(a)). The model is further simplified (Fig. 5(b)) by concentrating all of the axial-stress-carrying area of the matrix at an effective radius $\bar{R}$ between a and R, and assuming that the region in $a < r < \bar{R}$ supports only shear stresses $\tau_{rz}(r,z)$. The equilibrium and constitutive relations in this region simplify to

$$\frac{\partial\tau_{rz}}{\partial r} + \frac{\tau_{rz}}{r} = 0 \tag{19}$$

$$\tau_{rz} = G_m \frac{\partial w}{\partial r} \tag{20}$$

where $w(r,z)$ is the axial displacement, measured from the uncracked state. It follows that

$$\tau_{rz}(r,z) = \frac{a\tau_i(z)}{r} \tag{21}$$

where $\tau_i(z)$ is the interface shear stress, given by

$$\tau_i(z) = \frac{G_m(w_m - w_f)}{a \log(\bar{R}/a)} \tag{22}$$

in terms of the fiber and matrix displacements $w_f \equiv w(a,z)$ and $w_m \equiv w(\bar{R},z)$. Fiber equilibrium implies

$$\frac{\partial \sigma_f}{\partial z} + \left(\frac{2}{a}\right)\tau_i = 0 \tag{23}$$

and since the composite cylinder is isolated, Eq. (16) remains valid. Eliminating w_m and w_f from

$$\left.\begin{aligned} \frac{\sigma_f - \sigma_f^I}{E_f} &= \frac{dw_f}{dz} \\ \frac{\sigma_m - \sigma_m^I}{E_m} &= \frac{dw_m}{dz} \end{aligned}\right\} \tag{24}$$

and Eqs. (16), (22), (23), and applying the boundary conditions (17) and (13) at $z = 0$ and $|z| = \infty$ respectively leads to the following results for the downstream stresses:

$$\left.\begin{aligned} \sigma_f^D - \sigma_f^U &= (c_m/c_f)\sigma_m^U e^{-\rho|z|/a} \\ \sigma_m^D - \sigma_m^U &= -\sigma_m^U e^{-\rho|z|/a} \\ \tau_i^D &= \frac{z}{|z|}\frac{\rho}{2}(c_m/c_f)\sigma_m^U e^{-\rho|z|/a} \end{aligned}\right\} \tag{25}$$

where

$$\rho = \left[\frac{2G_m E}{c_m E_m E_f \log(\bar{R}/a)}\right]^{1/2} \tag{26}$$

If the fibers are held in the matrix by friction, this result is valid only if

the no-slip condition

$$\tau_s \geq \tau_i^D(0^+)$$

or

$$\sigma + (E/E_m)\sigma_m^I \leq \left[\frac{2c_f E}{\rho c_m E_m}\right]\tau_s \tag{27}$$

is met.

Slipping fibers

When the no-slip condition (27) is violated, frictional sliding between fiber and matrix, with $\tau_i = \tau_s$, occurs in a length ℓ_s on either side of the crack. Then Eqs. (16), (17) and (23) imply that

$$\left.\begin{aligned} \sigma_f^D &= \sigma/c_f - 2\tau_s|z|/a \\ \sigma_m^D &= 2(c_f/c_m)\tau_s|z|/a \\ \tau_i^D &= \tau_s \end{aligned}\right\} \tag{28}$$

for $0 \leq |z| \leq \ell_s$, far downstream from the crack tip. Re-solving Eqs. (16), (21)-(23), now with the boundary conditions $\tau_i = \tau_s$ at $|z| = \ell_s$ and, again, (13) at $|z| = \infty$, leads to

$$\left.\begin{aligned} \sigma_f^D - \sigma_f^U &= \frac{2\tau_s}{\rho} e^{-\rho(|z|-\ell_s)/a} \\ \sigma_m^D - \sigma_m^U &= -\frac{2\tau_s}{\rho}(c_f/c_m)e^{-\rho(|z|-\ell_s)/a} \\ \tau_i^D &= \frac{z}{|z|}\tau_s e^{-(|z|-\ell_s)/a} \end{aligned}\right\} \tag{29}$$

for $|z| \geq \ell_s$. Then imposition of the requirement that the axial stresses be continuous at $|z| = \ell_s$ provides the equation

$$\ell_s/a = \frac{\left[\sigma + (E/E_m)\sigma_m^I\right]\left[\frac{c_m E_m}{c_f E}\right]}{2\tau_s} - \frac{1}{\rho} \tag{30}$$

APPENDIX A

Estimate of Effective Radius $\bar{R}$ in Shear-Lag Model

Evaluation of the shearing energy contribution in Eq. (32) gives

$$\frac{2c_f(1+\nu_m)}{E_m} \log \bar{R}/a \int_{-\infty}^{\infty} \tau_i^2 dz \tag{A1}$$

This relates to the simplified model of Fig. 5(b), but now let us return to the configuration of Fig. 5(a), and contemplate a continuous shear lag model in which the matrix stress σ_m is distributed across the outer cylinder. Longitudinal equilibrium implies

$$r \frac{\partial \sigma_m}{\partial z} + \frac{\partial (r\tau_{rz})}{\partial r} = 0 \tag{A2}$$

together with the boundary conditions

$$\left.\begin{aligned} \tau_{rz}(a) &= \tau_i \\ \tau_{rz}(R) &= 0 \end{aligned}\right\} \tag{A3}$$

The assumed distribution

$$\tau_{rz}(r,z) = \frac{\tau_i(z)}{a} \left(\frac{c_f}{c_m}\right) \frac{R^2 - r^2}{r} \tag{A4}$$

satisfies these boundary conditions. Substitution into (A2) gives

$$\frac{\partial \sigma_m}{\partial z} = 2(c_f/c_m)(\tau_i/a) \tag{A5}$$

uniform in r, and this is consistent with the equilibrium requirements (23) and (16). Accordingly, an appropriate solution for the z-distributions of the stresses based on the principle of minimum complementary energy (which requires the use of an equilibrium approximation) based on the assumption (A4) is legitimate. Except for the definition of the characteristic parameter ρ, this solution will be identical to the one derived on the basis of the simplified model. The

propagation of matrix cracks into the fibers. The post-matrix-cracking strength exhibited in Fig. 1 and the accompanying pseudo-ductility, would then be lost.

ACKNOWLEDGEMENT

This work was initiated by the DARPA Materials Research Council under Contract MDA903-82-C-0428 with the University of Michigan, and was completed with support from the National Science Foundation under Grants DMR-83-16979 and MEA-82-13925, the Office of Naval Research under Contract N00014-84-K-0510, and the Divison of Applied Sciences, Harvard University.

REFERENCES

Aveston, J., Cooper, G. A. and Kelly, A. (1971), "Single and Multiple Fracture" in The Properties of Fibre Composites, Conference Proceedings, National Physical Laboratory, IPC Science and Technology Press Ltd., pp. 15-26.

Aveston, J. and Kelly, A. (1973), "Theory of Multiple Fracture of Fibrous Composites", Journal of Materials Science, 8, pp. 352-362.

Aveston, J. and Kelly A. (1980), "Tensile First Cracking Strain and Strength of Hybrid Composites and Laminates", Phil. Trans. R. Soc. Lond. A294, pp. 519-534.

Hannant, D. J., Hughes, D. C. and Kelly, A. (1983), "Toughening of Cement and Other Brittle Solids with Fibres", Phil. Trans. R. Soc. Lond. A310, pp. 175-190.

Kelly, A. (1976), "Composites with Brittle Matrices" in Frontiers in Materials Science (eds. L. E. Mura and C. Stein), Marcel Dekker, Inc., New York, pp. 335-364.

Marshall, D. and Evans, A. G. (1985), "Failure Mechanisms in Ceramic Fiber/Ceramic Matrix Composites", Journal of the American Ceramic Society, to be published.

Prewo, K. M. and Brennan, J. J. (1980), "High Strength Silicon Carbide Fiber Reinforced Glass Matrix Composites", Jour. Mater. Sci. 15, pp. 463-468.

$$\sigma_{cr} = \sigma_1 - \left(\frac{E}{E_m}\right)\sigma_m^I$$

Measured values of σ_{cr} gave

$$(\sigma_{cr})_{exp} = 290 \pm 20 \text{ MPa}$$

These results suggest the presence of a small initial axial compression. This is consistent with observations reported by Marshall and Evans (1985) of matrix crack closure, upon unloading, at small tensile loads. But initial axial compression in the matrix would ordinarily be accompanied by tension normal to the fiber-matrix interface. Accordingly, interfacial roughness rather than Coulomb friction may have been the primary source of the interface shear resistance in the Marshall-Evans experiments.

CONCLUDING REMARKS

The two idealized assumptions pursued herein concerning the fiber-matrix interface -- frictionally constrained, sliding fibers and initially bonded, debonding fibers -- are not, of course, exhaustive. Combinations of these possibilities could coexist, and interface roughness might play a more important role than interface pressure in providing slipping resistance. Two interesting, if tentative, conclusions can nevertheless be reached:

1. If Coulomb friction is operative, optimal strain mismatches exist that maximize the matrix cracking strength.
2. In the case of initially bonded fibers, a fairly small interface debonding toughness ($\mathcal{J}_d \sim \mathcal{J}_m/5$) suffices to inhibit debonding during the matrix cracking process.

A final cautionary note: the inhibition of either debonding or slipping may be quite undesirable despite the fact that the matrix cracking strength is thereby increased. Full maintenance of fiber-matrix continuity facilitates

and this condition will generally be easily met. This means that as a function of decreasing $(\mathcal{G}_d/\mathcal{G}_m)$, the matrix cracking strength will drop abruptly from its no-debond value when $(\mathcal{G}_d/\mathcal{G}_m)$ falls below its debond threshold value. This is illustrated in Fig. 12 for $E_f/E_m = 3$, $\nu_m = 1/4$, and $\sigma_m^I = 0$. It is interesting to note that once it drops from its no-debond value, σ_{cr} remains fairly insensitive to debond toughness until extremely low values of $\mathcal{G}_d$ are reached.

EXPERIMENTS

In some recent experiments, Marshall and Evans (1985) studied first-cracking in a ceramic system consisting of silicon-carbide fibers in a lithium-alumino-silicate glass matrix. The nominal values of pertinent parameters were

$$\left.\begin{aligned} c_f &= .5 \\ E_m &= 85\ GPa \\ E_f &= 200\ GPa \end{aligned}\right\} E = 142.5\ GPa$$

$$\nu_m = .25$$

$$a = 8.0\times10^{-6}\ m$$

$$K_m = 2.0\ MPa\text{-}m^{1/2}$$

$$\mathcal{G}_m = 44\ N/m \quad (= K_m^2(1-\nu_m^2)/E_m)$$

Push-through and indentation tests of individual fibers in composite samples gave measured values of $\tau_s \approx 2.0$ MPa, suggesting that the frictional-slip model should be applicable.

On the basis of the nominal data, Eqs. (38)-(40) give

$$\sigma_0 = 1625\ MPa \qquad (B = .88)$$

$$\sigma_1 = 265\ MPa$$

This puts $\sigma_1/\sigma_0 = .16$ well within the large-slip range (Fig. 7), and so the theoretical prediction for the cracking stress is

axis and each lower branch must be overcome. Since the debonded lengths along the lower branches are quite small, it seems reasonable to presume the presence of initial material flaws and imperfections that are equivalent to initially debonded regions of similarly small size. Then crack-tip stresses would push these effectively debonded lengths to the upper branches of the curves.

Threshold Bond Toughness

The function $Q(X)$ in Fig. 9 attains a maximum value $Q^* = 2.061$ at $X^* = .9204$. Since debonding can not occur for $Q > Q^*$, this critical value of Q can be used in Eq. (62b) to obtain, as a function of c_f, threshold values $(\mathcal{G}_d/\mathcal{G}_m)^*$ of the ratio of debonding to fracture toughness that would prevent debonding. The results, shown in Fig. 11, indicate that a debonding toughness that is quite small in comparison to matrix fracture toughness suffices to suppress crack-tip debonding over the practical range of fiber fraction.

Critical Cracking Stress

With the use of Eq. (36) for ρ, Eq. (55) for σ_{cr} becomes

$$\frac{\sigma_{cr}}{\sigma_0} + \frac{E}{E_m}\frac{\sigma_m^I}{\sigma_0} = \left\{ \frac{1 + \dfrac{4c_f}{c_m}\left(\dfrac{\ell_d}{a}\right)\left(\dfrac{\mathcal{G}_d}{\mathcal{G}_m}\right)}{1 + \dfrac{B^2}{c_m}\left[\dfrac{6E}{(1+\nu_m)E_f}\right]^{1/2}\left(\dfrac{\ell_d}{a}\right)} \right\}^{1/2} \tag{64}$$

where B (Fig. 6) is given by Eq. (39) as a function of c_f, and ℓ_d/a is defined as a function of c_f and $\mathcal{G}_d/\mathcal{G}_m$ by Eqs. (62) and the upper branch of the curve in Fig. 10. For $(\mathcal{G}_d/\mathcal{G}_m) > (\mathcal{G}_d/\mathcal{G}_m)^*$, no debonding occurs, and the old no-slip result $\dfrac{\sigma_{cr}}{\sigma_0} + \dfrac{E}{E_m}\dfrac{\sigma_m^I}{\sigma_0} = 1$ applies. When debonding does occur, we can expect the result (64) to provide a lower cracking strength than that for the no-debond case. For $(\mathcal{G}_d/\mathcal{G}_m) < (\mathcal{G}_d/\mathcal{G}_m)^*$, the right-hand side of (64) is certainly less than unity if

$$(\mathcal{G}_d/\mathcal{G}_m)^* < \frac{B^2}{4c_f}\left[\frac{6E}{E_f(1+\nu_m)}\right]^{1/2} \tag{65}$$

The solution of (59), with the boundary conditions $U(\pm \ell_d) = 0$, permits the calculation of the energy expression

$$V = \frac{1}{2}\int_0^{\ell_d} \sigma_r(z)U(z)dz \tag{60}$$

which represents the loss in potential energy of half of the loaded matrix jacket due to debonding. Then the energy-release-rate relation

$$2\pi a \mathcal{G}_d = \frac{\partial V}{\partial \ell_d} \tag{61}$$

provides the condition governing ℓ_d. The result (Appendix C) is the pair of parametric equations

$$\ell_d/a = (1+\sqrt{c_f})\left(\frac{1-\nu_m}{8c_f}\right)^{1/2} X \tag{62a}$$

$$\mathcal{G}_d/\mathcal{G}_m = \frac{(1+\sqrt{c_f})^3}{128\pi c_m}\left[\frac{2}{c_f(1-\nu_m)}\right]^{1/2} Q(X) \tag{62b}$$

relating ℓ_d/a to $\mathcal{G}_d/\mathcal{G}_m$, where

$$Q(X) = \left\{\frac{\int_0^X \frac{\cosh s\, ds}{\sqrt{s}}}{\cosh X}\right\}^2 \tag{63}$$

is plotted in Fig. 9.

Note that Eqs. (62) imply that ℓ_d/a is not a single-valued function of $\mathcal{G}_d/\mathcal{G}_m$. But from the energy-based derivation that led to this result, it follows that combinations of ℓ_d/a and $\mathcal{G}_d/\mathcal{G}_m$ associated with the region to the left of the curve in Fig. 9 are unstable, while those to the right are stable. The implications of this are better seen in Fig. 10, which show, as examples, explicit plots of ℓ_d/a vs. $\mathcal{G}_d/\mathcal{G}_m$ for several values of c_f. The upper part of each curve represents stable debonded lengths, but for debonding to occur at all an energy barrier associated with the region between the horizontal

Debond Length Analysis

We suppose that stress changes in the vicinity of the crack tip debond the fiber-matrix interface just ahead of the advancing crack for a distance ℓ_d on each side of the plane of the crack. To estimate ℓ_d we will again adopt a composite cylinder model in which we pretend that axisymmetric debonding is produced by an axisymmetric distribution of load applied to the matrix cylinder that jackets the fiber (Fig. 8). Conservatively, we take the magnitude of this loading as the stress

$$\sigma_r(z) = \frac{K_m}{4\sqrt{\pi|z|}} \tag{56}$$

and apply it at the mean radius R_m of the matrix jacket. Here $K_m = [E_m \mathcal{G}_m/(1-\nu^2)]^{1/2}$ is the critical elastic stress-intensity factor of the matrix, and (56) is just the asymptotic distribution of horizontal tension just above the crack tip. The debond length ℓ_d will be calculated on the basis of an energy balance involving the debonding toughness $\mathcal{G}_d$, and the energy changes in the matrix during debonding. The deformation of the matrix will be analyzed on the basis of thick-cylinder theory, in which only transverse shear stresses and circumferential tension resist radial displacement. In terms of the cylinder thickness

$$t = R - a = a(c_f^{-1/2}-1) \tag{57}$$

and the mean radius

$$R_m = \frac{1}{2}(R+a) = \frac{a}{2}(c_f^{-1/2}+1) \tag{58}$$

the differential equation governing the radial displacement $U(z)$ at $r = R_m$ is taken as

$$-G_m t \frac{d^2U}{dz^2} + \left[\frac{E_m t}{R_m^2(1-\nu_m^2)}\right] U = \sigma_r(z) \tag{59}$$

linear initial part of the curve in Fig. 7, justifying the use of Eq. (40) for σ_{cr} .

There is an interesting connection between Ω_{OPT} and the mismatch Ω_{SC} for self-cracking of the matrix in the absence of external stress. Under the assumption of large slip, self-cracking occurs when the right-hand side of (47) vanishes, which implies that

$$\Omega_{SC} = 3\sqrt{3}\ \Omega_{OPT} \tag{53}$$

MATRIX CRACKING: (ii) INITIALLY BONDED, DEBONDING FIBERS

Cracking Condition

We assume that there is initial transverse interface tension in the composite, so that downstream from the crack tip, regions of the fiber-matrix interface that have been debonded stay open.

The steady-state cracking condition (12) is then

$$\frac{1}{2}\int_{-\infty}^{\infty}\left\{\frac{c_f}{E_f}(\sigma_f^U-\sigma_f^D)^2+\frac{c_m}{E_m}(\sigma_m^U-\sigma_m^D)^2\right\}dz+\frac{1}{2\pi R^2 G_m}\int_{-\infty}^{\infty}\int_{a}^{\bar{R}}\left[\frac{a\tau_i^D}{r}\right]^2(2\pi r)drdz = c_m\mathcal{J}_m + 4c_f(\ell_d/a)\mathcal{J}_d \tag{54}$$

where we will use (13), (31) for $|z| < \ell_d$, and (25), with $|z|$ replaced by $(|z| - \ell_d)$, for $|z| > \ell_d$. (As before, we ignore transverse-stress contributions to strain energy.) This leads to the result

$$\frac{\sigma_{cr}}{\sigma_0} = \left\{\frac{1+\dfrac{4c_f}{c_m}\dfrac{\ell_d}{a}\dfrac{\mathcal{J}_d}{\mathcal{J}_m}}{1+\dfrac{\rho\ell_d}{a}}\right\}^{1/2} - \left(\frac{E}{E_m}\right)\frac{\sigma_m^I}{\sigma_0} \tag{55}$$

where ρ is given by (36), but now we require an estimate for the debond length ℓ_d .

are obtained.

If we anticipate that the optimum value of Ω will lead to large-slip matrix cracking, it is appropriate to use Eq. (40) for σ_{cr}, with $\tau_s = \mu q$ in Eq. (41). Then

$$\frac{\sigma_{cr}}{E} = \left[\frac{6\mu c_f^2 E_f \mathscr{E}_m}{c_m E_m E a}\right]^{1/3} \left(\frac{q}{E_m}\right)^{1/3} - \frac{\sigma_m^I}{E_m} \tag{47}$$

with q/E_m and σ_m^I/E_m given by (45). For $\Omega > 0$, σ_{cr} will attain a maximum value at $\Omega = \Omega_{OPT}$ when the condition

$$\left[\frac{6\mu c_f^2 E_f \mathscr{E}_m}{c_m E_m E a}\right]^{1/3} \left(\frac{q}{E_m}\right)^{1/3} = 3\left(\frac{\sigma_m^I}{E_m}\right) \tag{48}$$

is met. Hence

$$\Omega_{OPT} = \frac{\lambda_1 E(1-\nu_m)}{3E_f}\left[\frac{\mu \mathscr{E}_m}{\lambda_2^3 c_f E_m a}\right]^{1/2} \tag{49}$$

and

$$\left.\begin{aligned}(\sigma_{cr}/E)_{MAX} &= 2\left(\frac{\lambda_2}{\lambda_1}\right)\left(\frac{E_f}{E}\right)\left(\frac{c_f}{1-\nu_m}\right)\Omega_{OPT} \\ &= \frac{2}{3}\left[\frac{c_f \mu \mathscr{E}_m}{\lambda_2 E_m a}\right]^{1/2}\end{aligned}\right\} \tag{50}$$

At this optimum design, the associated slip length, based on the first term of Eq. (30), is given by

$$\ell_s/a = \frac{3\lambda_2 E_f}{\mu E} \tag{51}$$

Corroboration of the validity of the large-slip assumption follows from the observation that

$$\frac{(\sigma_{cr})_{MAX} + (E/E_m)\sigma_m^I}{\sigma_0} = \frac{1}{B}\left(\frac{c_m \mu}{\lambda_2}\right)^{1/2}\left[\frac{E(1+\nu_m)}{6E_f}\right]^{1/4} \tag{52}$$

at $\Omega = \Omega_{OPT}$. This value will generally be small enough to fall in the nearly

is valid for the sliding frictional resistance τ_s, it follows that increasing the strain mismatch would raise σ_1 as well as σ_m^I. Then Eq. (40) implies the existence of an optimal strain that maximizes the externally applied cracking stress σ_{cr}. (However, the assumption of Coulomb friction is not necessarily valid. Conceivably, τ_s may be due primarily to interface roughness, in which case the optimization study that follows is inapplicable.)

Suppose that non-elastic strains e_m and e_f occur isotropically in matrix and fiber during fabrication, and call

$$\Omega = (e_f - e_m)$$

the strain mismatch. (If, for example, the mismatch is due only to thermal strains, $\Omega = (\alpha_f - \alpha_m)\Delta T$, where ΔT is the temperature change, and α_m, α_f are the linear thermal expansions over the range ΔT. Note that Ω is positive if the matrix contracts more than the fiber during fabrication.)

For simplicity, we assume that both the fibers and the matrix are isotropic. A straightforward analysis of the composite cylinder model of Fig. 5(a) then gives

$$\left.\begin{aligned} \frac{q}{E_m} &= \frac{1}{2\lambda_1}\left[\frac{c_m}{1-\nu_m}\right]\Omega \\ \frac{\sigma_m^I}{E_m} &= \frac{\lambda_2}{\lambda_1}\left[\frac{E_f}{E}\right]\left[\frac{c_f}{1-\nu_m}\right]\Omega \end{aligned}\right\} \tag{45}$$

where λ_1, λ_2 are functions of c_f, E_f/E_m, ν_f, and ν_m shown explicitly in Appendix B. For $c_f \to 1$, $\lambda_1, \lambda_2 \to 1$, and both λ_1 and λ_2 will not vary too much from unity for reasonable values of c_f and E_f/E_m. If we assume $\nu_f = \nu_m = \nu$, the neat forms

$$\left.\begin{aligned} \lambda_1 &= 1 - \frac{1}{2}\left(\frac{1-2\nu}{1-\nu}\right)\left(1 - \frac{E}{E_f}\right) \\ \lambda_2 &= 1 - \frac{1}{2}(1 - E/E_f) = \frac{1}{2}(1 + E/E_f) \end{aligned}\right\} \tag{46}$$

$$Y \equiv \left(\frac{\sigma_{cr}}{E}+\frac{\sigma_m^I}{E_m}\right)\left(\frac{c_m E_m \rho}{2c_f \tau_s}\right) \tag{42}$$

the results can be manipulated into the form

$$\left.\begin{aligned}\frac{\sigma_{cr}+(E/E_m)\sigma_m^I}{\sigma_0} &= \left(\frac{Y}{3}\right)\left(\frac{\sigma_1}{\sigma_0}\right)^3 \\ \text{where}\qquad \left(\frac{\sigma_1}{\sigma_0}\right) &= \left(\frac{27}{Y^3+3Y-1}\right)^{1/6}\end{aligned}\right\} \tag{43}$$

In the range $Y>1$ specified by the slip condition (27), Eqs. (43) are parametric relations giving

$$\frac{(\sigma_{cr}+E/E_m)\sigma_m^I}{\sigma_0}$$

as the function of the independent variable (σ_1/σ_0) plotted in Fig. 7. For $Y=1$, $(\sigma_1/\sigma_0)=3^{1/3}=1.442$, and so for $(\sigma_1/\sigma_0)>3^{1/3}$, the no-slip result

$$\frac{\sigma_{cr}+(E/E_m)\sigma_m^I}{\sigma_0}=1$$

applies. For $Y\to\infty$, $(\sigma_1/\sigma_0)\to 0$, and $\sigma_{cr}+(E/E_m)\sigma_m^I$ approaches the large-slip ACK value σ_1. This large-slip result is a good approximation over the substantial initial portion of the curve in Fig. 7 that is nearly linear. In the slipping range, the slip length ℓ_s may be found from Eq. (30).

Optimal Strain Mismatch

Mismatches between the non-elastic fiber and matrix strains that occur during fabrication (e.g., due to cooling, plasticity, creep, or phase transformation) will produce initial matrix stresses σ_m^I as well as fiber-matrix interface pressure q, and a positive q will generally go along with positive σ_m^I. If a Coulomb friction law of the form

$$\tau_s = \mu q \tag{44}$$

where

$$\frac{\sigma_0}{E} = B\left[\frac{6c_f^2 E_f}{c_m^2 E(1+\nu_m)}\right]^{1/4}\left[\frac{\mathcal{J}_m}{aE_m}\right]^{1/2} \tag{38}$$

When the estimate (34) is used for $\log \bar{R}/a$, we have

$$B = \left[\frac{2c_m^3}{-6 \log c_f - 3c_m(3-c_f)}\right]^{1/4} \tag{39}$$

Then $B \to 1$ for $c_f \to 1$, and, as shown in Fig. 6, B does not vary much from unity over a large range of fiber concentration c_f.

The ACK results for slipping fibers (Aveston et al., 1972) can be recovered from Eq. (32) by substituting Eqs. (28) for σ_f^D and σ_m^D in $|z| < \ell_s$; dropping the shear contribution to the energy; neglecting <u>all</u> energy contributions in $|z| > \ell_s$; and dropping the $(1/\rho)$ term from the formula (30) for ℓ_s/a. (It can be verified that these truncations are all asymptotically valid for $\ell_s/a \to \infty$.) The result is

$$\frac{\sigma_{cr}}{E} + \frac{\sigma_m^I}{E_m} = \frac{\sigma_1}{E} \tag{40}$$

where

$$\frac{\sigma_1}{E} = \left[\frac{6c_f^2 E_f \tau_s}{c_m E_m E}\right]^{1/3}\left[\frac{\mathcal{J}_m}{aE_m}\right]^{1/3} \tag{41}$$

is equivalent to the ACK expression for the critical, large-slip cracking strain. (Aveston et al. do not actually present a counterpart to Eq. (40); they derive the cracking criterion $\sigma_{cr}/E = \sigma_1/E$ for $\sigma_m^I = 0$, and separately, also deduce that $\sigma_m^I/E = \sigma_1/E$ is the condition for self-cracking in the absence of external loading.)

To bridge between the no-slip and large-slip ACK results, we can substitute the full expressions (29) for $|z| \geq \ell_s$, together with (28) for $|z| \leq \ell_s$, into (32). With Y defined by

$$\frac{1}{2}\int_{-\infty}^{\infty}\left[\frac{c_f}{E_f}(\sigma_f^U-\sigma_f^D)^2+\frac{c_m}{E_m}(\sigma_m^U-\sigma_m^D)^2\right]dz+\frac{1}{2\pi R^2 G_m}\int_{-\infty}^{\infty}\int_{a}^{\bar{R}}(\tau_{rz}^D)^2\,2\pi r dr dz = c_m \mathcal{G}_m \qquad (32)$$

wherein, by Eq. (21), $\tau_{rz}^D = \frac{a}{r}\tau_i^D$. (Here we neglect contributions to strain energy associated with downstream changes in transverse stress.) For the no-slip case substitution of Eqs. (25) into (32) leads to the formula

$$\frac{\sigma_{cr}}{E}+\frac{\sigma_m^I}{E_m}=\left[\frac{c_f E_f \mathcal{G}_m \rho}{a E_m E}\right]^{1/2} \qquad (33)$$

for the cracking stress σ_{cr} . Except for the initial-stress term σ_m^I/E_m , this is essentially the result originally given by Aveston and Kelly (1973) for no-slip matrix cracking.

Aveston and Kelly do not specify $\bar{R}$ in the definition (26) for ρ , beyond the unelaborated statement that $\bar{R}$ is equal to the radius at which the matrix displacement equals its average value. On a different basis, the explicit estimate

$$\log \bar{R}/a = -\frac{2\log c_f + c_m(3-c_f)}{4c_m^2} \qquad (34)$$

is derived in Appendix A. (This gives $(\bar{R}-a)/(R-a)\to 1/3$ for $c_f\to 1$; for $c_f\to 0$, $(\bar{R}-a)/(R-a)\to e^{-3/4}=.47$.) If we introduce the utility constant

$$B=\left[\frac{c_m}{6\log \bar{R}/a}\right]^{1/4} \qquad (35)$$

into the definition of ρ , we get

$$\rho=\frac{B^2}{c_m}\left[\frac{6E}{E_f(1+\nu_m)}\right]^{1/2} \qquad (36)$$

and we can rewrite (33) in the convenient form

$$\frac{\sigma_{cr}}{E}+\frac{\sigma_m^I}{E_m}=\frac{\sigma_0}{E} \qquad (37)$$

for the slip length. For $\ell_s = 0$ this is consistent with the no-slip requirement (27), and Eqs. (28), (29) are, of course, valid only for $\ell_s/a \geq 0$. For ℓ_s larger than a few fiber radii, the contribution to ℓ_s/a of the term $(1/\rho)$ in (30) will be small.

Initially bonded, debonding fibers

Now we suppose that debonding along a length ℓ_d on either side of the crack is produced near the crack tip by interface fracture, and that the debonded regions remain open downstream of the crack tip. The axial and shear stresses in $0 \leq |z| \leq \ell_d$ are simply

$$\left.\begin{aligned} \sigma_f^D &= \sigma/c_f \\ \sigma_m^D &= 0 \\ \tau_i^D &= 0 \end{aligned}\right\} \tag{31}$$

and for $|z| \geq \ell_d$ shear-lag analysis reproduces the results (25) from the no-slip case, with $|z|$ in the exponents simply replaced by $(|z| - \ell_d)$. We presume that the interface shear stresses will not produce any additional debonding that increases ℓ_d beyond its crack-tip value.

Note that in contrast to the case of frictionally slipping fibers, the shear-lag solution for debonded fibers involves a discontinuity in τ_i at $|z| = \ell_d$.

MATRIX CRACKING: (i) UNBONDED, FRICTIONALLY CONSTRAINED FIBERS

Critical Cracking Stress

Using the stresses of the shear-lag model in the steady-state cracking equation (11) gives (for $L \to \infty$)

correspondence between the two solutions is easily found by replacing $\bar{R}$ by R in the shear energy contribution in Eq. (32) and using (A4) for τ^D_{rz}. This gives

$$\frac{2(1+\nu_m)}{E_m}\left(\frac{c_f}{c_m}\right)^2\left[\left(\frac{R}{a}\right)^2 \log\frac{R}{a}+1-\frac{3}{4}\left(\frac{R}{a}\right)^2-\frac{1}{4}\left(\frac{a}{R}\right)^2\right]\int_{-\infty}^{\infty}\tau_i^2 dz \qquad (A6)$$

With $(R/a)^2 = (1/c_f)$, comparison of (A1) and (A6) then provides the estimate (34) for $\bar{R}/a$.

APPENDIX B

Initial Stresses

By the classical Lamé solution for the unloaded composite cylinder of Fig. 5(a), the initial circumferential stresses $\sigma_{\theta f}$ and $\sigma_{\theta m}$ in the fiber and matrix at their interface are

$$\left.\begin{aligned} \sigma_{\theta f} &= -q \\ \sigma_{\theta m} &= q(1+c_f)/c_m \end{aligned}\right\} \tag{B1}$$

where q is the interface pressure. The conditions of interface strain continuity are

$$\left.\begin{aligned} \frac{1}{E_m}[\sigma_m^I - \nu_m(\sigma_{\theta m}-q)] + e_m &= \frac{1}{E_f}[\sigma_f^I - \nu_f(\sigma_{\theta f}-q] + e_f \\ \frac{1}{E_m}[\sigma_{\theta m} - \nu_m(\sigma_m^I-q)] + e_m &= \frac{1}{E_f}[\sigma_{\theta f} - \nu_f(\sigma_f^I-q)] + e_f \end{aligned}\right\} \tag{B2}$$

Substitution of (B1), elimination of σ_f^I via Eq. (15), and solution for σ_m^I and q gives the results (45) of the text, with λ_1 and λ_2 defined by

$$\lambda_1 = \frac{1-(1-E/E_f)(1-\nu_f)/2+c_m(\nu_m-\nu_f)/2-(E/E_f)[\nu_f+(\nu_m-\nu_f)c_fE_f/E]^2}{(1-\nu_m)\Delta} \tag{B3}$$

$$\lambda_2 = \frac{[1-(1-E/E_f)/2](1+\nu_f)+(1+c_f)(\nu_m-\nu_f)/2}{\Delta} \tag{B4}$$

where

$$\Delta = 1 + \nu_f + (\nu_m-\nu_f)c_fE_f/E \tag{B5}$$

and E is given by (14). Setting $\nu_m = \nu_f$ gives Eqs. (46).

APPENDIX C

Debond-Length Analysis

Letting

$$\left.\begin{aligned} z &= \ell_d(\zeta/X) \\ U &= \frac{1}{4}\left[\frac{\mathcal{G}_m(1-\nu^2)}{\pi E_m}\right]^{1/2}\left[\frac{R_m^{3/2}}{t}\right]\left[\frac{2}{1-\nu}\right]^{1/4} u \end{aligned}\right\} \tag{C1}$$

where

$$X = (\ell_d/R)\left(\frac{2}{1-\nu}\right)^{1/2} \tag{C2}$$

reduces the differential equation (59) to

$$-u_{\zeta\zeta} + u = |\zeta|^{-1/2} \tag{C3}$$

and the boundary conditions become $u(\pm X) = 0$. The energy-release-rate condition (61) becomes

$$\mathcal{G}_d = \left(\frac{\mathcal{G}_m}{32\pi}\right)\left(\frac{R_m^2}{at}\right)\left(\frac{2}{1-\nu}\right)^{1/2}\int_0^X \zeta^{-1/2}\left(\frac{\partial u}{\partial X}\right)d\zeta \tag{C4}$$

For $\zeta > 0$, the solution of Eq. (C3) is

$$u = -\int_0^\zeta \frac{\sinh(\zeta-\zeta')d\zeta'}{\sqrt{\zeta'}} + \frac{\cosh\zeta}{\cosh X}\int_0^\zeta \frac{\sinh(X-\zeta')d\zeta'}{\sqrt{\zeta'}} \tag{C5}$$

which gives

$$\frac{\partial u}{\partial X} = \frac{\cosh\zeta}{\cosh^2 X}\int_0^X \frac{\cosh\zeta'd\zeta'}{\sqrt{\zeta'}} \tag{C6}$$

Then (C4) provides the results (62), (63) of the text, when c_f is introduced via Eqs. (57), (58).

For calculation purposes, the function $Q(X)$ in Eq. (63) may be written in terms of Dawson's integral

$$D(Z) = e^{-Z^2} \int_0^Z e^{s^2} ds \tag{C7}$$

which is tabulated and available in software. Thus

$$Q(X) = \left[\frac{e^X D(X^{1/2}) + \frac{\sqrt{\pi}}{2} \operatorname{erf}(X^{1/2})}{\cosh X} \right]^2 \tag{C8}$$

where $\operatorname{erf}(Z) = \frac{2}{\sqrt{\pi}} \int_0^Z e^{-s^2} ds$. For X large, $Q \sim 1/X$, and for X small, $Q \sim 4X$.

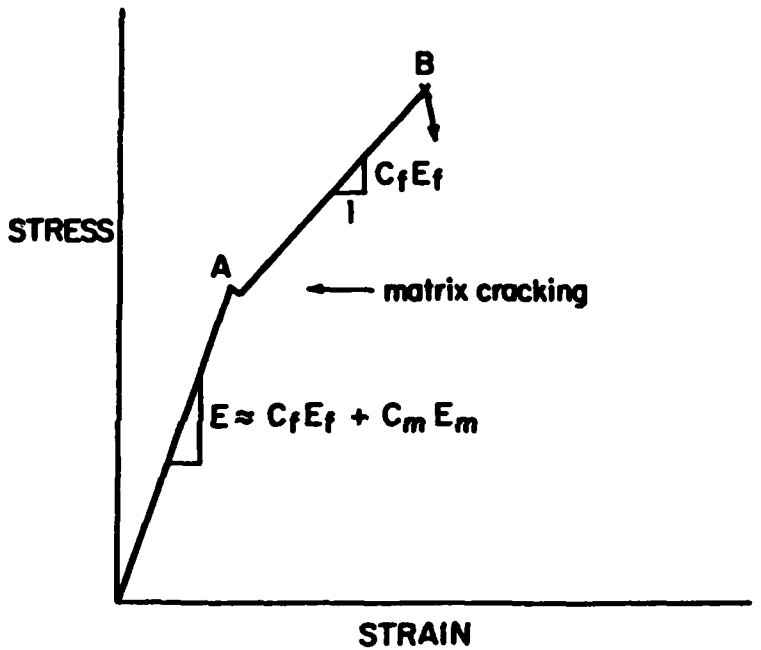

Fig. 1 Schematic stress-strain curve of brittle-matrix fibrous omposite.

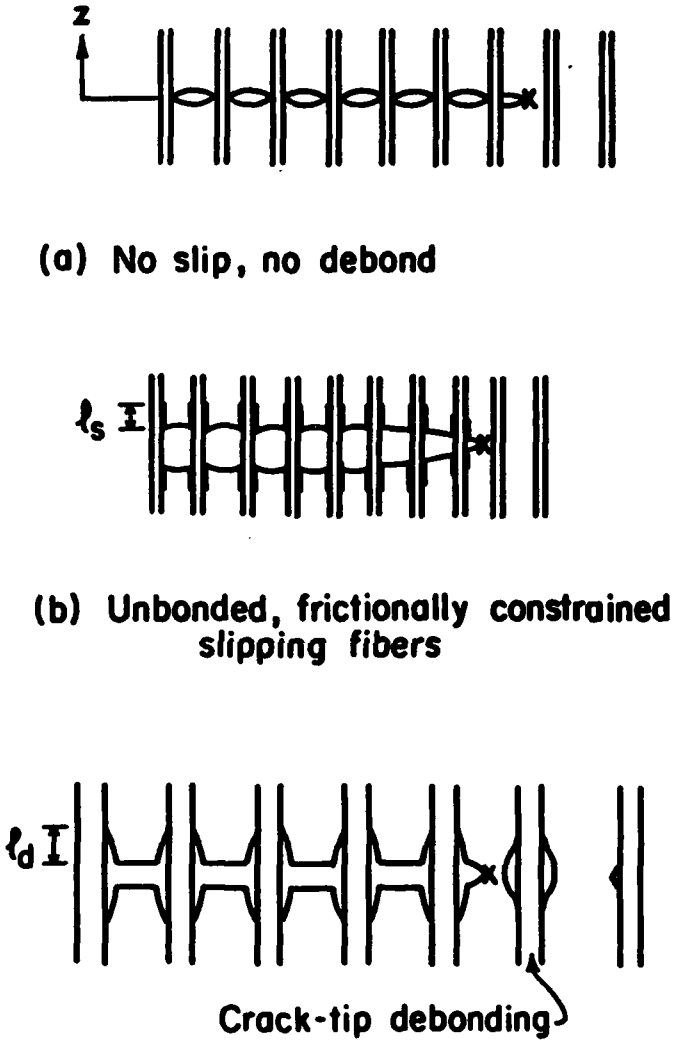

(a) No slip, no debond

(b) Unbonded, frictionally constrained slipping fibers

(c) Initially bonded, debonding fibers

Fig. 2 Steady-state matrix cracking.

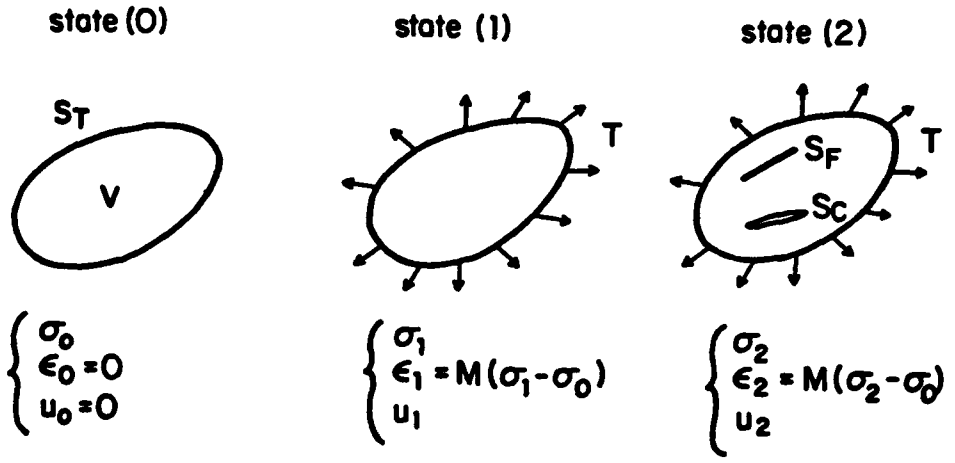

Fig. 3 Three successive states: (0) unloaded, prestressed, (1) loaded, (2) new open crack surface S_C, more sliding on surface S_F.

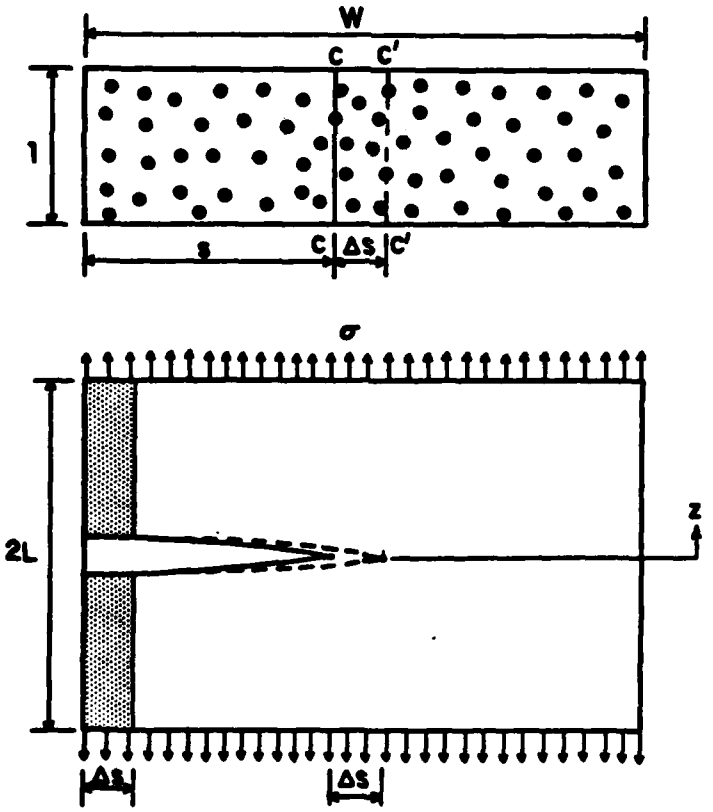

Fig. 4 Advancing matrix crack.

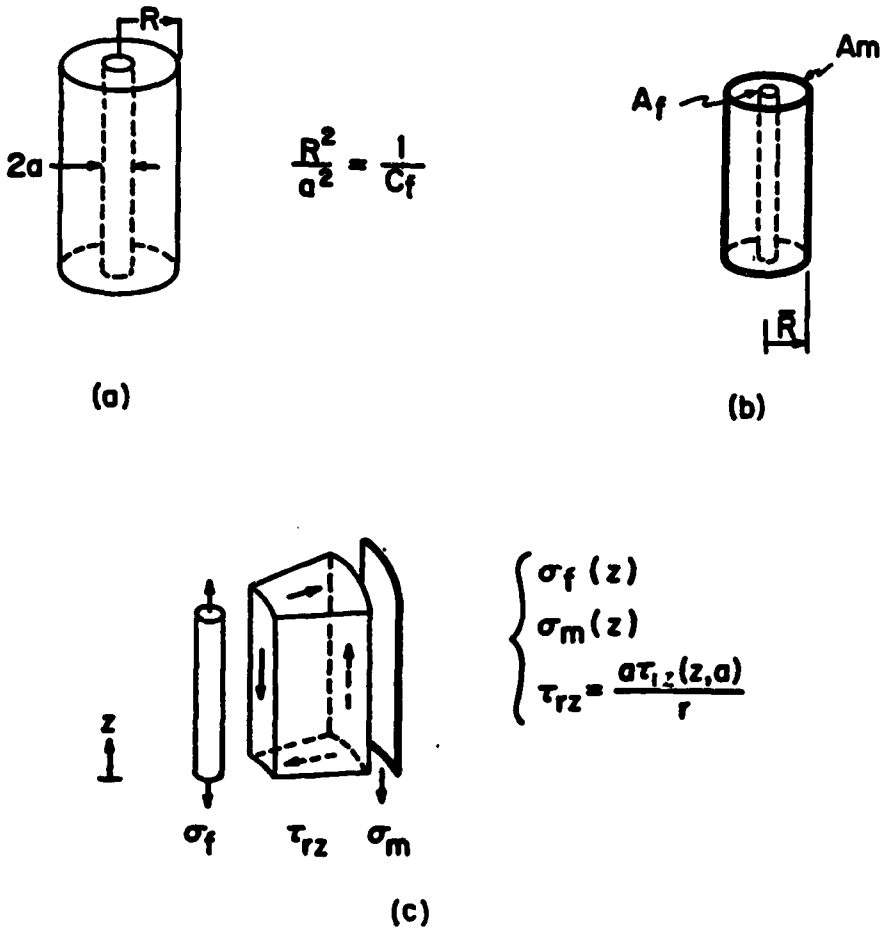

Fig. 5 Shear-lag model (a) composite cylinder, (b) concentrated matrix area at effective radius $\bar{R}$, (c) axial and shear stresses.

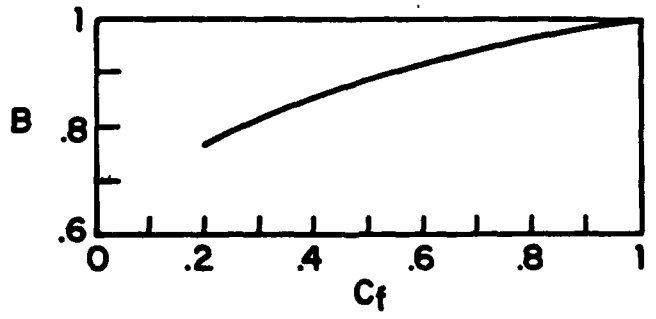

Fig. 6 Utility constant B in $\sigma_0/E = B\left[\frac{6c_f^2E_f}{c_m^2E(1+\nu_m)}\right]^{1/4}\left[\frac{\delta_m}{aE_m}\right]^{1/2}$.

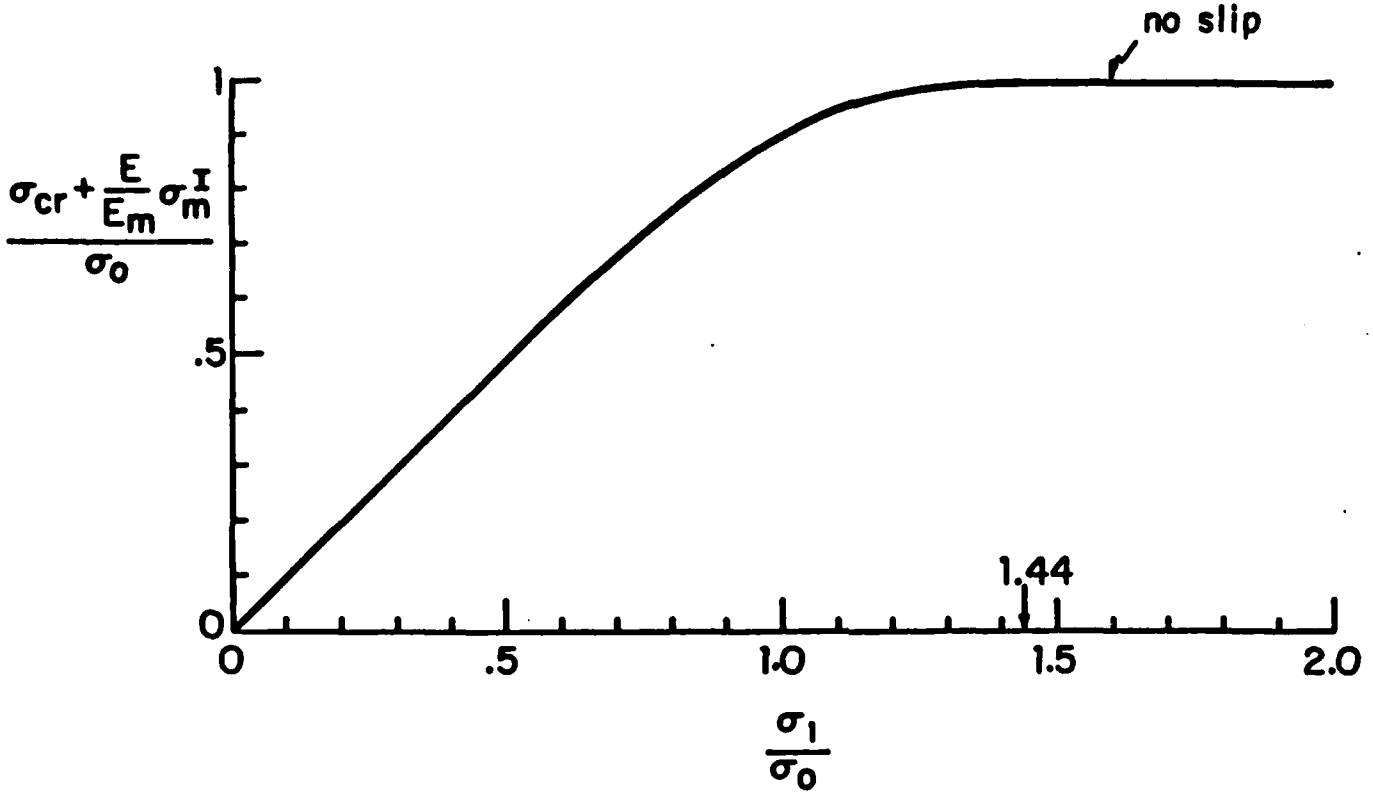

Fig. 7 Matrix cracking stress, initially unbonded, frictionally constrained fibers;

$$\sigma_0/E = B\left[\frac{6c_f^2 E_f}{c_m^2 E(1+\nu_m)}\right]^{1/4}\left[\frac{\mathcal{J}_m}{aE_m}\right]^{1/2}, \quad \sigma_1/E = \left[\frac{6c_f^2 E_f \tau_s}{c_m E E_m}\right]^{1/3}\left[\frac{\mathcal{J}_m}{aE_m}\right]^{1/3}.$$

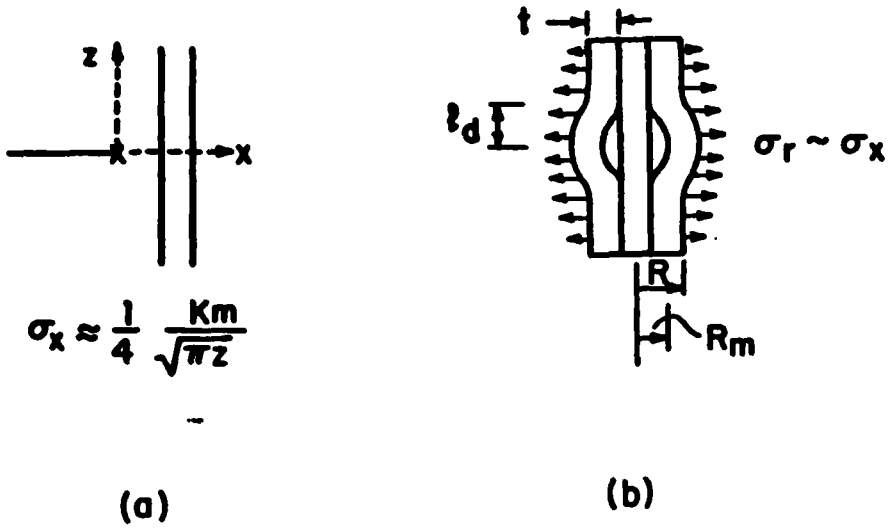

Fig. 8 Debonding model (a) crack tip stress, (b) thick-cylinder model.

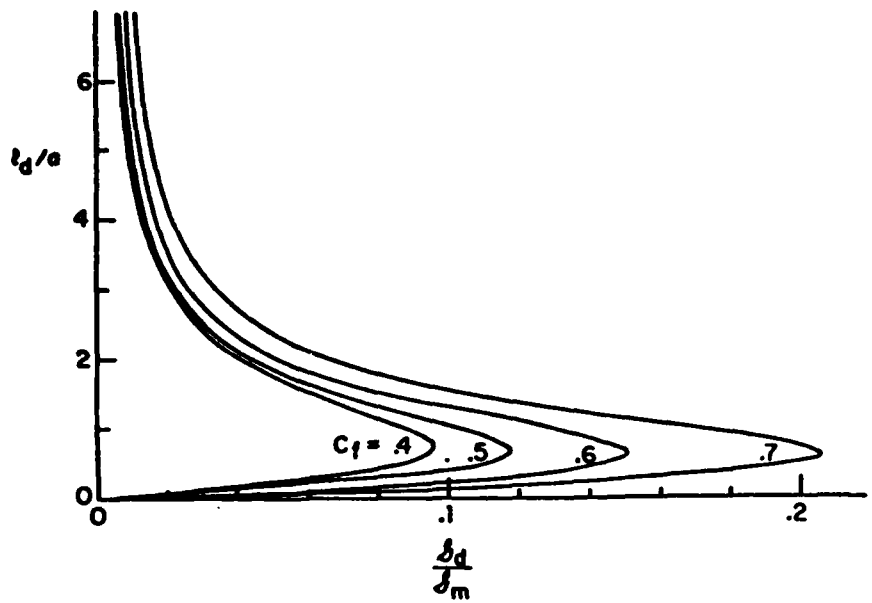

Fig. 10 Debond length versus debond-toughness/matrix-toughness ratio ($\nu_m = 1/4$).

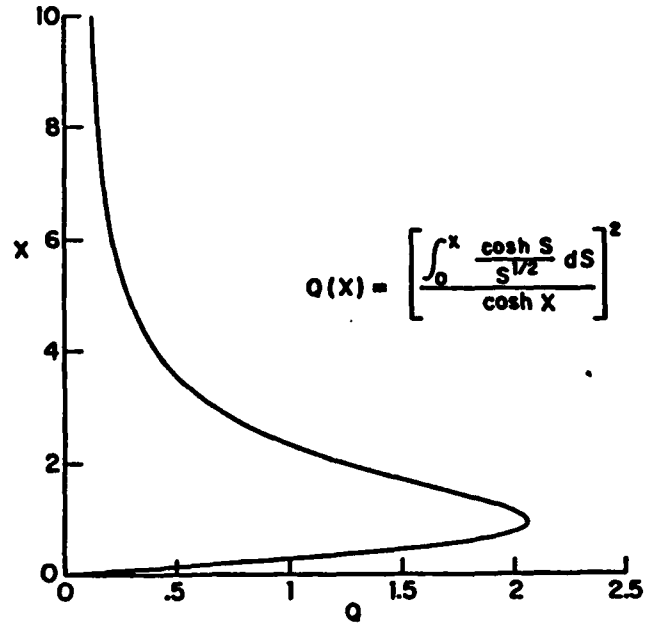

Fig. 9 Debond length versus debond toughness, universal nondimensional representation

$$\ell_d/a = (1+\sqrt{c_f})\left(\frac{1-\nu_m}{8c_f}\right)^{1/2} X ,$$

$$\mathcal{G}_d/\mathcal{G}_m = \frac{(1+\sqrt{c_f})^3}{128\pi c_m}\left|\frac{2}{c_f(1-\nu)_m}\right|^{1/2} Q(X)$$

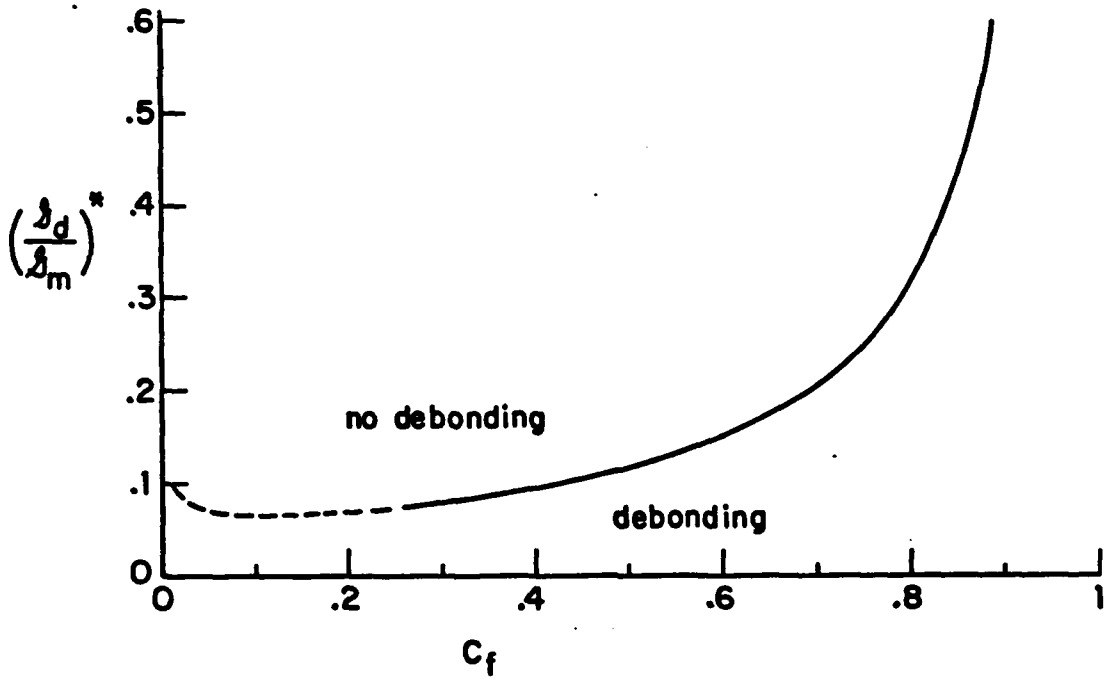

Fig. 11 Threshold bond toughness ($\nu_m = 1/4$) .

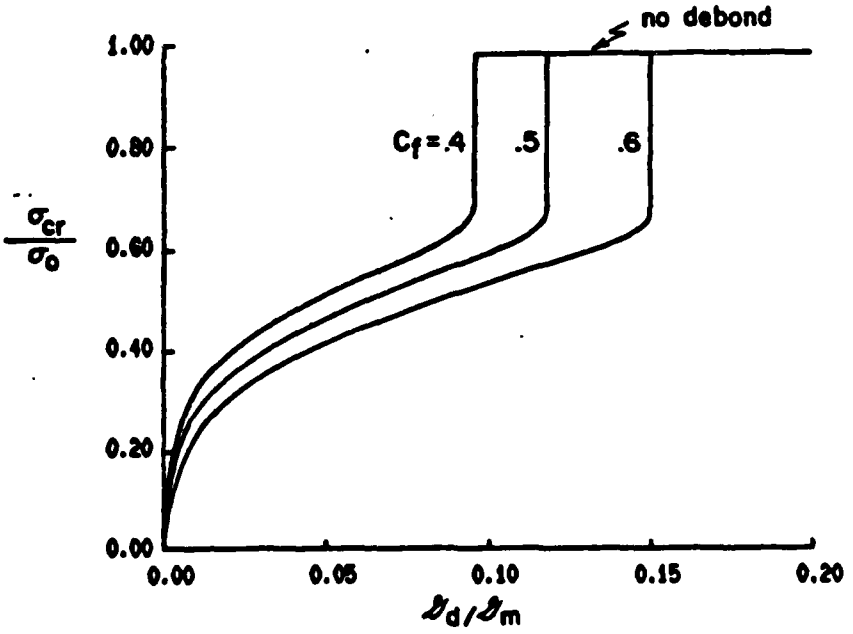

Fig. 12 Matrix cracking strength versus debond toughness/matrix toughness ratio; illustrative example $E_f/E_m = 3$, $\nu_m = 1/4$, $\sigma_m^I = 0$.

END

FILMED

7-85

DTIC